

¹⁸F-FPEB, a PET Radiopharmaceutical for Quantifying Metabotropic Glutamate 5 Receptors: A First-in-Human Study of Radiochemical Safety, Biokinetics, and Radiation Dosimetry

Dean F. Wong¹⁻⁴, Rikki Waterhouse⁵, Hiroto Kuwabara¹, Jongho Kim¹, James R. Brašić¹, Wichana Chamroonrat¹, Michael Stabins⁶, Daniel P. Holt¹, Robert F. Dannals¹, Terence G. Hamill⁷, and P. David Mozley⁷

¹Russell H. Morgan Department of Radiology and Radiological Science, Johns Hopkins University School of Medicine, Baltimore, Maryland; ²Department of Psychiatry, Johns Hopkins University School of Medicine, Baltimore, Maryland; ³Department of Neuroscience, Johns Hopkins University School of Medicine, Baltimore, Maryland; ⁴Department of Environmental Health Sciences, Johns Hopkins University School of Medicine, Baltimore, Maryland; ⁵Pfizer Inc., New York, New York; ⁶Vanderbilt University, Nashville, Tennessee; and ⁷Merck Research Laboratories, West Point, Pennsylvania

Identification of safe and valid PET radioligands for metabotropic glutamate receptor, type 5 (mGluR5), is essential to measure changes in brain mGluR5 in neuropsychiatric disorders, to confirm central mGluR5 occupancy of drug candidates, and to guide dose selection for obtaining an optimum therapeutic window. Here we present the results of a first-in-human study assessing the safety and effectiveness of a novel PET radiopharmaceutical, ¹⁸F-3-fluoro-5-[(pyridin-3-yl)ethynyl]benzonitrile (¹⁸F-FPEB), for quantifying regional brain concentrations of mGluR5. **Methods:** Quantification of whole-body biokinetics was conducted in 6 healthy adults (3 men and 3 women). The radiation safety profile was estimated with OLINDA/EXM software. Subsequently, pairs of dynamic brain scans were obtained for 11 healthy men to identify optimal methods for derivation of regional distribution volume and binding potential and to determine the repeatability of measurement. **Results:** The whole-body effective radiation dose was approximately 17 μ Sv/MBq (62 mrem/mCi), with the gallbladder receiving the highest dose of 190 μ Sv/MBq. In brain studies, time-activity curves showed high accumulation in the insula/caudate nucleus, moderate uptake in the thalamus, and the lowest concentration in the cerebellum/pons. The plasma reference graphical analysis method appeared optimal for ¹⁸F-FPEB; it showed acceptable test-retest variability of nondisplaceable binding potential (<10%) and identified the highest nondisplaceable binding potential values (from ~0.5 in the globus pallidus to ~3.5 in the insula) for target regions. Safety assessments revealed no clinically meaningful changes in vital signs, electrocardiogram, or laboratory values. **Conclusion:** ¹⁸F-FPEB is safe and well tolerated, and its regional cerebral distribution is consistent with previous reports in the literature for metabotropic glutamate receptors. The repeatability of

measurement suggests that ¹⁸F-FPEB is suitable for quantifying mGluR5 in humans.

Key Words: positron emission tomography (PET); neuroreceptors; metabotropic glutamate receptor subtype 5 (mGluR5); 3-fluoro-5-[(pyridin-3-yl)ethynyl]benzonitrile (FPEB); ¹⁸F-FPEB; radioligand; human radiation dosimetry

J Nucl Med 2013; 54:1-9

DOI: 10.2967/jnumed.112.107995

Metabotropic glutamate receptors offer a plausible alternative to ionotropic receptors for drug development, as they are involved in most aspects of normal brain function through the modulation of synaptic transmission and cell excitability (1,2). Specifically, metabotropic glutamate receptor, type 5 (mGluR5), seems to be an important regulator of the glutamatergic system because of its hypothesized involvement in anxiolytic, antidepressant, and antiaddictive effects; memory processes; and neurotransmitter release (3). Thus, several pharmaceutical companies have focused significant resources on the development of drugs to act directly at, or modulate, mGluR5; the clinical use of these drugs, however, could be limited by central side effects such as amnesia and psychotomimetic symptoms (4-7). A clinically established PET radiotracer would be valuable for demonstrating differences in brain mGluR5 expression in healthy individuals and patients, for confirming central occupancy of novel mGluR5 drug candidates, and for guiding dose selection.

The preclinical evaluation of several recently developed mGluR5 radiotracers (8-11) supports mGluR5 as a quantifiable target by PET in mice and nonhuman primates. One such radiotracer was ¹⁸F-3-fluoro-5-[(pyridin-3-yl)ethynyl]benzonitrile (¹⁸F-FPEB), a potent, selective mGluR5 inhibitor with excellent properties as a central nervous system

Received May 8, 2012; revision accepted Jul. 27, 2012.

For correspondence or reprints contact: Dean F. Wong, 601 N. Caroline St., JHOC Room 3245, Johns Hopkins Medical Institutions, Baltimore, MD 21287-0807.

E-mail: dfwong@jhmi.edu

Published online ■■■■.

COPYRIGHT © 2013 by the Society of Nuclear Medicine and Molecular Imaging, Inc.

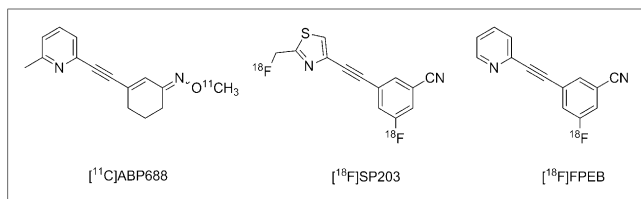


FIGURE 1. Structures of radiolabeled mGluR5 antagonists.

ligand (12). ¹⁸F-FPEB is a low-molecular-weight radiotracer made at high specific activity that selectively labels mGluR5 in vitro and in vivo and provides high-quality mGluR5-specific images in rhesus monkey PET studies (12). PET imaging with ¹⁸F-FPEB results in a large, long-lived specific signal with the highest uptake in the caudate and lowest uptake in the cerebellum in nonhuman primates, consistent with autoradiographic results for mGluR5 receptors (12). These data strongly indicate that ¹⁸F-FPEB is a suitable candidate for further clinical development. Two other radiolabeled mGluR5 antagonists, ¹¹C-ABP688 and ¹⁸F-SP203 (13,14), have been evaluated in humans.

[Fig. 1] Figure 1 shows the chemical structure of these radioligands and ¹⁸F-FPEB.

This study included an initial whole-body (WB) study to define the tissue and organ radiation dose associated with a single intravenous administration of ¹⁸F-FPEB. The study also developed a method of dynamic brain imaging with test–retest reliability-of-measurement analyses. The paradigm of dynamic PET imaging of the human brain facilitated the validation of ¹⁸F-FPEB for quantifying mGluR5 by characterizing its regional kinetics and its ability to generate robust outcome measures of nondisplaceable binding potential (BP_{ND}) and distribution volumes (V_T).

We report here the first human study designed with the following goals in view: demonstrate the clinical and radiation tolerability of ¹⁸F-FPEB, with the hypothesis that it is entirely safe for human use; demonstrate dynamic human brain and plasma metabolites, with the hypothesis that they are feasible for human studies; and initially quantify human brain mGluR5, with the hypothesis that binding is consistent with the known metabotropic glutamate receptor regional distribution and that test–retest reliability is good.

MATERIALS AND METHODS

Subjects, Eligibility, and Overall Study Design

This was an open-label, 2-part, first-in-human pilot study conducted under an exploratory U.S. investigational new drug application that included and followed animal toxicology and safety studies of the unlabeled imaging agent and initial non-human radiation dosimetry performed at Merck Research Laboratories (15). All procedures were approved by the Johns Hopkins Medicine Institutional Review Board, and all participants signed informed consent forms.

A contract research organization, Parexel, Inc., accrued and medically managed the research subjects. A total of 17 (14 men and 3 women) nonsmoking healthy volunteers participated after demonstrating good physical and mental health, as determined by

medical history, physical examination, vital signs, clinical laboratory tests, and a 12-lead electrocardiogram. Of these subjects, 6 (3 men and 3 women; mean age ± SD, 35 ± 7 y) participated in the radiation dosimetry study, and the remaining 11 men (mean age, 42 ± 7 y) participated in the brain imaging study.

To be included, the participants had to be subjectively healthy, have a body mass index of 19–29 kg/m², be shorter than 195 cm (6 ft 5 in), and, if a woman, have a negative pregnancy test. Subjects were excluded from participation if they had any physical or mental disease or condition; were taking a medication that could interfere with the safety, tolerability, or biokinetics of the tracer; or, in part 2, failed to complete the MR head scan.

Participants in part 1, the WB radiation dosimetry study, received a single administration of ¹⁸F-FPEB. They were inpatients at the Parexel clinical research center and then underwent a single PET/CT scan consisting of 8–9 bed positions at the Johns Hopkins University PET Center.

Participants in part 2 were also inpatients. They received 2 administrations of ¹⁸F-FPEB on different days within 16 d (range, 2–16 d), except for 1 subject. After each administration, dynamic brain scans were acquired for 90 min, with arterial and venous blood sampling for metabolite and input functions.

Chemical Structure and Radiosynthesis of ¹⁸F-FPEB

¹⁸F-FPEB was synthesized at high specific activity using a slight modification of a published method (12); the modification involved using isocratic preparative high-pressure liquid chromatography (HPLC) and cesium carbonate instead of potassium/Kryptofix (Merck). After production of ¹⁸F-fluoride, target water was passed through a Chromafix 30-PS-HCO₃ QMA cartridge (Macherey-Nagel GmbH and Co.) to trap the ¹⁸F-fluoride. The cartridge was eluted with aqueous cesium carbonate and then acetonitrile into a glass reaction vessel. The ¹⁸F-fluoride and cesium carbonate solution was azeotropically dried with multiple additions of acetonitrile at 120°C under a nitrogen flow. A dimethyl sulfoxide solution of FPEB precursor was added to the reaction vessel and microwaved for 4 min at 50 W. The mixture was diluted with water and applied to a semipreparative HPLC column (XBridge Prep OBD, C18, 5 μm, 19 × 50 mm; Waters) and eluted with 30% acetonitrile:70% H₂O triethylamine buffer at pH 7.2 at an initial flow rate of 5 mL/min for the first 2 min and then 15 mL/min until product was observed and collected.

The ¹⁸F-FPEB fraction was collected in water and loaded onto a C18 Sep-Pak (Waters) and washed with 10 mL of 0.9% NaCl. The ¹⁸F-FPEB was eluted with 1 mL of ethanol followed by 10 mL of 0.9% NaCl, via a sterilizing 0.22-μm filter, into a sterile vial containing 4 mL of 0.9% NaCl.

¹⁸F-FPEB was demonstrated to meet all quality control criteria for a PET radiotracer including appropriate visual appearance and pH, radionuclidic, chemical, and radiochemical purities. The final radiotracer product was shown to be sterile and nonpyrogenic and lacking the presence of residual organic solvents from its preparation.

Clinical Safety Assessments

The safety and tolerability of ¹⁸F-FPEB was assessed and monitored through clinical and laboratory safety evaluations, including physical examinations, frequent vital sign measurements, 12-lead electrocardiograms, and relevant laboratory tests (hematology, chemistry, and urinalysis). For women, a urine pregnancy test for exclusion criteria was also conducted before any PET or MR

scan. The patient was followed up by telephone at about 72 h and 14 d after administration of ^{18}F -FPEB. In the dosimetry study, WB PET scans were used to estimate radiopharmaceutical biokinetics and regional radiation exposure. The outcome measures included effective dose and absorbed radiation doses to individual organs.

Effective dose was defined in 1991 by the International Commission on Radiological Protection in its publication 60 (16). Effective dose is calculated by summing the “tissue-weighting factor”-weighted organ-absorbed doses, which are a function of their assumed relative radiosensitivity for expressing carcinogenesis or genetic defects. The tissue-weighting factor given in publication 60 was a revision of that given in publication 26.

WB Imaging, Dosimetry, and Subject Exposure Estimates for ^{18}F -FPEB

Before the radiation dosimetry studies of ^{18}F -FPEB, tracer biodistribution data from PET in 3 male and 2 female rhesus monkeys were used to forecast the initial human radioactivity dose administered for the WB human biokinetic studies (15). The single-study dosage limit for men and women was based on the calculated dose to the upper large intestine, which appeared to receive the highest dose per administration in nonhuman primates. The maximum single-study activity of 185 MBq (5 mCi) was estimated to provide an exposure of 33 mGy and 37 mGy (per injection) to the upper large intestine of men and women, respectively, and 2.5 mGy per WB study. The maximum amount of ^{18}F -FPEB administered was set at 2 scans with approximately 185 MBq (5 mCi) to limit exposure to the large intestine, which was predicted to be the dose-limiting organ.

The subjects were positioned supine in a Discovery VCT PET/CT scanner (lutetium yttrium orthosilicate PET with a 15.7-cm axial field of view; GE Healthcare). To correct for photon absorption and scatter, as well as to provide anatomic information as a reference, a low-dose CT scan (64 slices; pitch, 0.984; tube voltage, 120 kVp; tube current, 20–200 mA; rotation time, 0.5 s) was performed before tracer administration. After intravenous injection of a mean of 188 MBq (range, 178–197 MBq) of ^{18}F -FPEB through an indwelling catheter, a series of 4 sequential WB PET scans (bed position overlap, 11 slices (36 mm); coincidence window, 6.5 ns; random correction, singles; energy window, 425–650 keV) were obtained at 4 time points (0, 10, 30, and 60 min). The duration of the dosimetry scans lasted approximately 105 min when there were 9 bed positions.

Each scan covered the body from the head to the mid thigh and consisted of 8–9 bed positions scanned for 1 min ($\times 8 = 8$ min), 2 min ($\times 8 = 16$ min), 3 min ($\times 8 = 24$ min), and 5 min ($\times 8 = 40$ min) in 3-dimensional mode. The data were then reconstructed in a 128×128 matrix (slice thickness, 3.75 mm) and corrected for photon attenuation and scatter using information from the corresponding CT scan.

Curve fits extrapolated to a time of infinity were used to calculate the time–activity integrals. The OLINDA/EXM program (17) was used to estimate the absorbed radiation doses. The effective dose served as the primary measure of radiation safety.

Brain Imaging Study and Reconstruction

MR Imaging. Participants who underwent dynamic brain PET also underwent structural MR imaging of the brain. All imaging was done on a 3-T Magnetom Trio scanner (Siemens Medical Solutions) equipped with the 3T Head Matrix Coil. T1-MPRAGE (magnetization-prepared 180° radio-frequency pulses and rapid gradient-echo) and

T2-weighted images were acquired, with all brain images read by an attending neuroradiologist to rule out clinical pathology.

PET Procedures. All brain-only scans were obtained on the second-generation High-Resolution Research Tomograph (CPS Innovations, Inc.), a lutetium oxyorthosilicate-based 2.5-mm-resolution dedicated brain PET scanner. Subjects had 1 venous catheter for the radioligand and 1 arterial catheter for input functions. The subjects were positioned in the scanner with their heads restrained by a custom-made thermoplastic mask. A 6-min transmission scan was acquired using a rotating ^{137}Cs source for attenuation correction. Dynamic PET acquisition was performed in 3-dimensional list mode for 90 min after an intravenous bolus injection of ^{18}F -FPEB. Arterial blood samples were collected, and selected samples were analyzed by HPLC for radioactive metabolites.

Reconstruction. High-Resolution Research Tomograph dynamic PET images were reconstructed using an iterative ordered-subset expectation maximization algorithm with 6 iterations, 16 subsets, data mashing (span) of 3, a maximum ring difference of 67, and corrections for attenuation, scatter, and dead time. This is the standard reconstruction algorithm for the High-Resolution Research Tomograph. The reconstructions were performed on a specialized 32-node (64 processors) cluster (IBM). The following 30-frame schedule was used from the list-mode collection: four 15-s, four 30-s, three 1-min, two 2-min, five 4-min, and twelve 5-min frames, for the 90-min scan.

Blood Sampling and Plasma Metabolite Collection

Total Radioactivity Plasma Curve. Arterial plasma samples (1.5 mL) were withdrawn manually at approximately 5, 10, 15, 20, 25, 30, 35, 40, 45, 50, 55, 60, 65, 70, 75, 80, 85, 90, 95, 100, 105, and 110 s and at 3, 4, 5, 8, 10, 15, 20, 30, 40, 60, 80, and 90 min; counted in a γ -counter; and cross-calibrated with the PET scanner.

^{18}F -FPEB Metabolites. Additional 6-mL radial arterial samples taken at 0, 2, 5, 10, 20, 30, 60, and 90 min for assessing the fraction of unchanged ^{18}F -FPEB in plasma were analyzed by HPLC using a general method developed for PET radioligands (18).

PET Data Analysis

WB Dosimetry Study. The injected dose of radioactivity was determined by dose calibrator after subtraction of the residual syringe activity. Because no voiding occurred during the WB scans, the entire injected activity was recovered in the PET/CT measures. Segmentations of each organ for volumes of interest (VOIs) were performed by a threshold method implemented with a Johns Hopkins University tool based on MATLAB (MathWorks) that allowed voxels with radioactivity above the current threshold to be displayed in a color map and then segmented into a VOI after elimination of unwanted connections to the other organs in all orthogonal slices (transverse, sagittal, and coronal). For the liver, cerebral cortex, bone marrow, spleen, thyroid, lung, heart, and kidneys, the optimum threshold was applied to the single time frame that most clearly showed the organ. The resulting VOIs were transferred to the remaining frames. For the urinary bladder, gallbladder, stomach, and small intestine, VOIs were determined on more than a single frame. The VOIs were applied to generate time–activity curves for a total of 12 organs. The standardized uptake values of each organ were calculated by dividing the measured activity concentration (Bq/mL) by the injected activity (Bq) per gram of body weight and then expressed as a percentage (i.e., definition of percentage standardized uptake value).

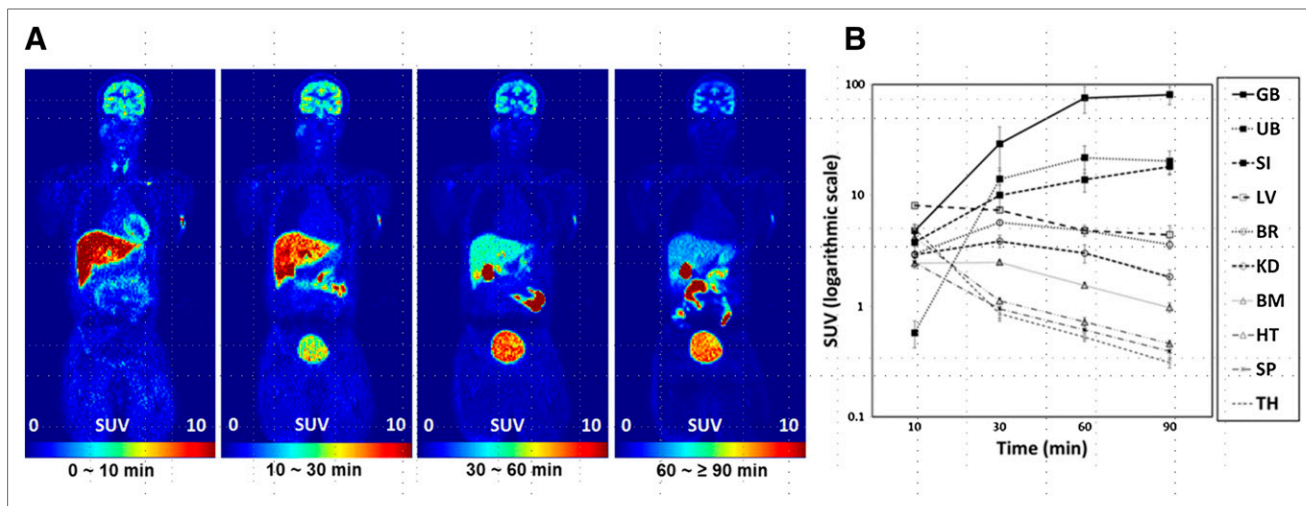


FIGURE 2. (A) ^{18}F -FPEB WB PET images 0–10, 10–30, 30–60, and 60–90 min after injection of 33-y-old man (73 kg) with 177.6 MBq (4.8 mCi) with specific activity of 555 GBq (15.0 Ci)/ μmol and FPEB mass of 0.07 μg . Gallbladder was critical organ for ranges of percentage standardized uptake value (SUV), decay-corrected to individual scan start times but not to injection time. Images are displayed using same scale for direct comparison of percentage SUV between images. (B) Tissue time–activity curves of non–decay-corrected ^{18}F activity using SUVs for various organs. Values are mean (\pm SEM) SUVs. GB = gallbladder; UB = urinary bladder; SI = small intestine; LV = liver; BR = brain; KD = kidney; BM = bone marrow; HT = heart; SP = spleen; TH = thyroid.

The percentage injected activity per organ was multiplied by reference standard organ masses (19), divided by the amount of activity administered, and then fit using SAAM II software (20). Time integrals of activity were entered into OLINDA/EXM software (version 1.1) (17) using the adult male model.

Accumulation of activity was observed in the bladder and integrated until 100 min, when accumulation was assumed to be negligible. The number of disintegrations in the remainder of the body was assumed to be equal to 100% of the activity administered, integrated to total decay of ^{18}F minus the disintegrations in other body organs. The observed bladder doses were integrated since no voiding occurred, which probably yielded conservative dose estimates.

Brain Imaging Study. Cortical VOIs were automatically defined using Freesurfer software (21) and combined into standard regions, including frontal, temporal, parietal, and occipital cortices; fusiform gyrus; cingulate; and insula. Subcortical regions were defined with FIRST software (22) and manually adjusted on individual MR images. Subcortical regions included putamen, caudate nucleus, globus pallidus, thalamus, hippocampus, and amygdala. VOIs were transferred from MR images to PET spaces following the MR imaging–to–PET coregistration parameters given by SPM5 (23,24) to obtain time–activity curves.

Mathematic Kinetic Modeling

We prespecified that the study would identify the compartmental model that most precisely described the kinetics of ^{18}F -FPEB in the brain using metabolite-corrected plasma time–activity curves. We expected that the V_T of the nondisplaceable compartment (25) could be estimated accurately in cerebellum (8,26,27) or in white matter (12) for radioligands of mGluR5.

A set of standard plasma input methods was used to identify the optimal method for derivation of V_T for ^{18}F -FPEB. The following 4 methods were tested: a 1-tissue-compartment model with 3 parameters (K_1 and k_2' , defined by Koeppe et al. (28), and v_0 , the tissue vascular volume); 2-tissue-compartment models with 5 parameters (K_1 , k_2 , k_3 , k_4 , and v_0 , defined by Innis et al. (25)), with

and without constraining the K_1/k_2 ratio (nondisplaceable V_T (28)) to the cerebellum estimate (TTCM and TTCM-C, respectively); and plasma reference graphical analysis (PRGA) (30). In TTCM and TTCM-C, BP_{ND} was given as the k_3/k_4 ratio. In the data analyses, metabolite-corrected plasma time–activity curves were obtained by applying the metabolite-corrected input function, given by HPLC analysis, to total plasma time–activity curves after interpolating at plasma sample times using the piecewise cubic Hermite interpolation implemented in MATLAB.

BP_{ND} maps were generated using PRGA, spatially normalized to a SPM5 standard brain using SPM5 (23), and averaged across subjects to generate averaged BP_{ND} maps of ^{18}F -FPEB.

Test–Retest Repeatability of Dynamic Brain Scans

Regional test–retest variability was calculated as follows and expressed as a percentage:

$$\text{Test–retest variability} = \sum_{i=1}^n \frac{|\text{test} - \text{retest}|}{\frac{\text{test} + \text{retest}}{2}} \cdot \frac{1}{n}, \quad \text{Eq. 1}$$

where test and retest stand for V_T or BP_{ND} of the test and retest scans, respectively, and n is the number of participants. We prespecified that ^{18}F -FPEB would be adequately qualified as a ligand for mGluR5 if test–retest variability were no more than 10%, commonly accepted for validity of PET radiotracers (31–36). We also analyzed the test–retest V_T and BP_{ND} using intraclass correlations in SPSS and tested agreement of BP_{ND} and V_T maps with regional distributions of mGluR5 (8,12,37).

RESULTS

Radiochemical Yield at End of Synthesis

The mean (\pm SEM) radiochemical yield was 1.7 ± 0.292 GBq (45.6 ± 7.39 mCi), and the mean specific activity at the end of synthesis was $6,000 \pm 823$ GBq/ μmol (16.2 ± 2.2 Ci/ μmol).

TABLE 1

Output from OLINDA for Residence Times of ¹⁸F-FPEB from WB PET Images

Source organ	¹⁸ F-FPEB residence time (h)
Brain	0.1092 ± 0.0430
Gallbladder contents	0.1147 ± 0.1307
Lower large intestine	0.0117 ± 0.0031
Small intestine	0.1164 ± 0.0312
Upper large intestine	0.0638 ± 0.0171
Heart wall	0.0039 ± 0.0022
Kidneys	0.0137 ± 0.0067
Liver	0.2820 ± 0.2269
Bone marrow	0.0197 ± 0.0186
Spleen	0.0014 ± 0.0006
Thyroid	0.0003 ± 0.0001
Urinary bladder	0.1080 ± 0.0687
Remainder	1.8333 ± 0.3920

Data are mean ± SD (n = 6).

Subjects

WB Radiation Dosimetry Study. Three men and 3 women (mean age ± SD, 35 ± 7 y; range, 24–45 y) were scanned on the Discovery VCT. The mean (±SD) ¹⁸F-FPEB dose was 188 ± 7 MBq (5.08 ± 0.18 mCi), with a mass of 0.10 ± 0.06 µg, specific activity of 5.3 × 10⁵ ± 2.9 × 10⁵ MBq/µmol, and a mass dose of 1.57 ± 0.96 pg/kg.

The free fraction was determined using methods developed by Hamill et al. (12). Plasma protein binding of ¹⁸F-FPEB was evaluated at tracer levels in human plasma. All calculations of protein binding were corrected for nonspecific binding of the tracer to the centrifugal filters. The average free fraction was determined to be 8.10% ± 0.67%, ensuring delivery of tracer to the brain.

Brain ¹⁸F-FPEB PET Study. For the first scan, the 11 subjects were given an average dose (±SD) of 181 ± 14 MBq (4.90 ± 0.38 mCi), with a mass of 0.15 ± 0.10 µg, specific activity of 3.7 × 10⁵ ± 2.3 × 10⁵ MBq/µmol, and a mass dose of 1.8 ± 1.3 pg/kg. For the second scan, the average dose was 179 ± 4 MBq (4.85 ± 0.11 mCi), with a mass of 0.23 ± 0.19 µg, specific activity of 2.9 × 10⁵ ± 1.9 × 10⁵ MBq/µmol, and a mass dose of 2.7 ± 2.5 pg/kg.

The dose, mass, and specific activity of test and retest scans were not statistically different (P > 0.1, paired t test). Means ± SDs for both test and retest scans were as follows: dose of 181 ± 10 MBq (4.88 ± 0.28 mCi), mass of 0.19 ± 0.15 µg, specific activity of 3.3 × 10⁵ ± 2.1 × 10⁵ MBq/µmol (8,963 ± 5,683 mCi/µmol), and mass dose of 2.2 ± 1.96 pg/kg.

Test–retest evaluation was performed for only 5 subjects because of technical problems with the HPLC (4 scans), uncorrectable head motion (1 scan), and withdrawal from the retest scan (1 subject). A total of 16 successful scans (i.e., those without the aforementioned problems) from 11 subjects (thus denoted as n = 11) were used for method evaluation and derivation of regional V_T and BP_{ND}.

Safety

There were no significant changes in vital signs, laboratory values, or electrocardiograms during the PET scans that could be attributed to the radiotracer. Mean systolic blood pressure was 122 mm Hg (maximum, 147 mm Hg), mean diastolic blood pressure was 68 mm Hg (maximum, 93 mm Hg), and mean heart rate was 64 beats/min (maximum, 92 beats/min). Mean QTc was 397 ms. (QTc is the QT interval corrected for heart rate, used to assess the risk for tachyarrhythmia. Normal QTc is ≤400 ms.) No subjects experienced more than a 28-ms change from baseline in QTc, and no QTc values were greater than 441 ms.

Absorbed Doses for WB Radiation Dosimetry

Coronal WB PET images are shown in Figure 2A. The mean number of disintegrations (Bq-h/Bq administered) of ¹⁸F-FPEB (n = 6) calculated from WB PET images are summarized in Table 1. All ¹⁸F-FPEB data were well fit with 1 or 2 exponential functions. The mean radiation dose estimates (n = 6) in the various organs is reported in Table 2. Most organs received exposures of about 7.7–44 µSv/MBq (28–160 mrem/mCi). VOI analyses of an average time–activity curve of non–decay–corrected ¹⁸F-FPEB (n = 6)

TABLE 2

Output from OLINDA for Radiation Doses of ¹⁸F-FPEB from PET Images and OLINDA/EXM

Target organ	¹⁸ F-FPEB radiation dose	
	µSv/MBq	mrem/mCi
Adrenals	13.9 ± 1.5	51.6 ± 5.5
Brain	20.2 ± 6.8	74.6 ± 25.1
Breasts	8.1 ± 0.9	29.9 ± 3.4
Gallbladder wall	191.4 ± 210.4	708.1 ± 708.1
Lower large intestine wall	21.1 ± 4.6	78.1 ± 17.2
Small intestine	40.0 ± 11.7	147.8 ± 43.3
Stomach wall	12.9 ± 0.5	47.7 ± 1.9
Upper large intestine wall	44.4 ± 13.1	164.3 ± 48.5
Heart wall	9.9 ± 1.5	36.7 ± 5.5
Kidneys	17.3 ± 5.6	64.0 ± 20.9
Liver	41.1 ± 28.2	152.1 ± 104.4
Lungs	10.3 ± 0.7	38.0 ± 2.8
Muscle	10.4 ± 0.9	38.6 ± 3.3
Ovaries	16.5 ± 2.3	61.0 ± 8.6
Pancreas	15.4 ± 1.9	56.9 ± 6.9
Red marrow	11.6 ± 1.0	43.0 ± 3.7
Osteogenic cells	15.7 ± 1.4	58.1 ± 5.1
Skin	7.7 ± 0.9	28.5 ± 3.5
Spleen	8.3 ± 0.8	30.8 ± 3.0
Testes	9.8 ± 1.5	36.2 ± 5.4
Thymus	9.6 ± 1.3	35.7 ± 4.9
Thyroid	8.0 ± 0.7	29.6 ± 2.8
Urinary bladder	52.3 ± 12.2	175.2 ± 77.0
Uterus	16.9 ± 1.9	62.5 ± 6.9
Total body	12.0 ± 0.2	44.4 ± 0.6
Equivalent dose	30.9 ± 13.1	114.4 ± 48.6
Effective dose	16.9 ± 1.8	62.4 ± 6.8

Data are mean ± SD.

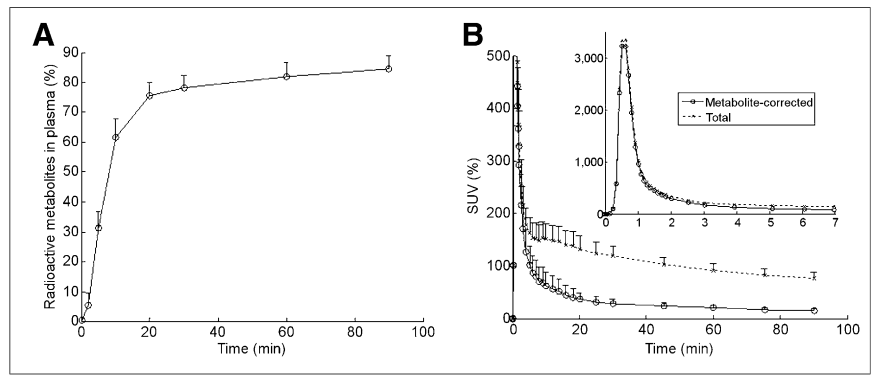


FIGURE 3. Line plots (means with SD bars, $n = 11$) of total radioactive metabolite fractions in plasma (A), and total and metabolite-corrected plasma time-activity curves expressed in standardized uptake value (SUV) (B). Inset shows first 7 min to visualize initial portions of time-activity curves.

revealed that most of the ^{18}F activity was seen in the hepatobiliary transit through the liver and gallbladder into the small intestine, with gradual retention of radioactivity in the urinary bladder (Fig. 2B). The gallbladder received the highest radiation dose, approximately $190 \mu\text{Sv}/\text{MBq}$ ($708 \text{ mrem}/\text{mCi}$). The urinary bladder received approximately $52 \mu\text{Sv}/\text{MBq}$ ($1,790 \text{ mrem}/\text{mCi}$). The effective dose was approximately $17 \mu\text{Sv}/\text{MBq}$ ($62 \text{ mrem}/\text{mCi}$).

Dynamic Brain Imaging and mGluR5 Quantification

Radioactive Metabolites and Plasma Time-Activity Curves. Total radioactive metabolites were about 60% at 10 min after injection, about 80% at 30 min, and about 5% at the end of the scan (90 min) (Fig. 3). Plasma time-activity curves peaked within 1 min of injection and decreased monotonically (Fig. 3).

Figure 4 Tissue Time-Activity Curves. Figure 4 shows decay-corrected tissue time-activity curves in percentage standardized uptake value for selected brain regions. Time-activity curves of good-retention regions (e.g., insular cortex and caudate nucleus) peaked at around 20 min and then gradually declined. Time-activity curves of medium-retention regions (e.g., thalamus) peaked within 10 min of the injection and declined monotonically. Time-activity curves of low-retention regions (e.g., cerebellum and pons) peaked within 10 min of injection and decreased monoexponentially.

Selection of Methods for PET Outcome Variables. Akaike information criteria (38) supported TTCM-C over a 1-tissue-compartment model in all brain regions, including the pons, which showed the lowest accumulation of radioactivity. TTCM yielded relatively unstable estimates of V_T at 60 min in time-consistency tests ($y = 1.1x - 1.1$; $R^2 = 0.964$, where x and y stand for V_T values given by PET frames 0 to 90 and 60 min, respectively), compared with TTCM-C and PRGA. Therefore, TTCM might not be appropriate for 90-min scans. TTCM-C and PRGA showed comparable results in time consistency tests for V_T (TTCM-C: $y = 1.0x - 0.51$, $R^2 = 0.987$; PRGA: $y = 1.0x - 0.86$, $R^2 = 0.988$) and for BP_{ND} (TTCM-C: $y = 1.0x - 0.08$, $R^2 = 0.964$; PRGA: $y = 1.0x - 0.01$, $R^2 = 0.986$). Therefore, it appeared that 60 min could be sufficient for TTCM-C and PRGA to yield stable estimates of V_T and BP_{ND} (and thus could be considered a time to reach steady state). The cerebellum was used for the V_T of

the nondisplaceable compartment for TTCM-C, whereas the pons was used to calculate BP_{ND} with PRGA because it showed the lowest V_T among tested regions.

Test-Retest Variability. TTCM-C and PRGA showed similar test-retest variability estimates of V_T across regions (Fig. 5A). Test-retest variability estimates were lower than 20% in most regions except for the caudate nucleus. Test-retest variability estimates of BP_{ND} were less than the 10% criterion in all regions (Fig. 5B), except for the globus pallidus. PRGA showed slightly better test-retest variability on BP_{ND} across regions than did TTCM-C (paired t test: $t_{12} = -4.9613$, $P < 0.001$). Intraclass correlation coefficients for test-retest across regions were as follows: TTCM-C V_T was 0.96 and BP_{ND} was 0.82; PRGA V_T was 0.96 and BP_{ND} was 0.91.

Regional V_T and BP_{ND} Values. Regional V_T and BP_{ND} are shown in Figure 6. V_T , which includes not only binding but also blood-brain transport properties, was a secondary variable for ^{18}F -FPEB because PRGA yielded robust estimates of BP_{ND} . Insula, temporal, and cingulate cortices showed high BP_{ND} values that could be visually identified on averaged BP_{ND} maps (Fig. 7).

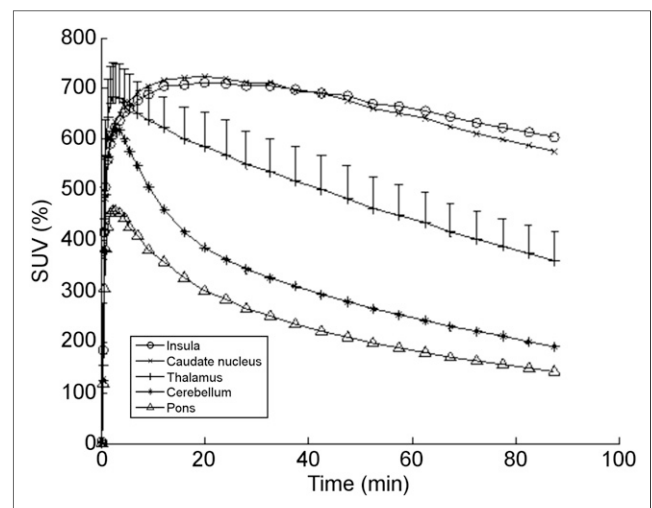


FIGURE 4. Average percentage standardized uptake value time-activity curves for ^{18}F -FPEB ($n = 11$) of representative regions. Data for thalamus include SD bars (SD in thalamus is representative of magnitude of error for all regions).

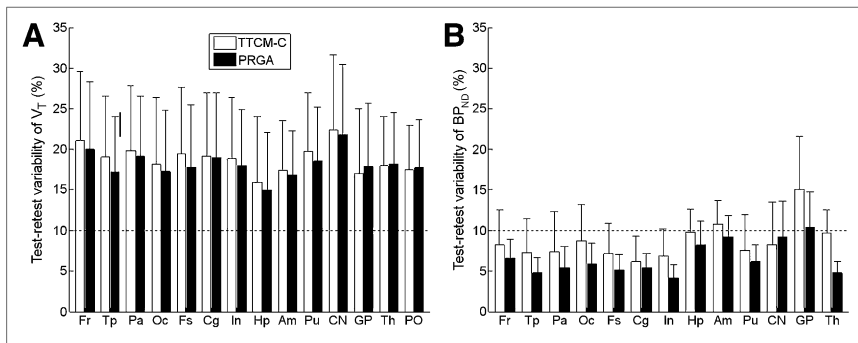


FIGURE 5. Histograms (means with SE bars) of regional estimates of test-retest variability (Eq. 1) for V_T (A) and BP_{ND} (B) given by TTCM-C and PRGA. The 10% level, which is the generally accepted criterion for acceptable reproducibility, is shown by horizontal dotted line. Fr = frontal lobe; Tp = temporal lobe; Pa = parietal lobe; Oc = occipital lobe; Fs = fusiform gyrus; Cg = cingulate gyrus; In = insula; Hp = hippocampus; Am = amygdala; Pu = putamen; CN = caudate nucleus; GP = globus pallidus; Th = thalamus; PO = pons.

DISCUSSION

The present study confirmed that PET imaging with ^{18}F -FPEB, prepared in high radiochemical yield and purity (12), seems safe and feasible for use in humans. The organ and effective doses were lower than those of our preclinical study (15); nonhuman primates had higher doses to the intestinal walls and testes and a lower dose to the gallbladder wall than did these human participants.

^{18}F -FPEB has low radiation doses (16.9 $\mu\text{Sv}/\text{MBq}$), comparable to clinically used ^{18}F -ligands such as ^{18}F -FDG (19–24 $\mu\text{Sv}/\text{MBq}$) (39).

The total radiation dose for an ^{18}F -FPEB administered activity of about 185 MBq (5 mCi) per scan for 3 scans is about 9.4 mSv (0.93 rem). The addition of about 12 mSv (1.20 rem) from the CT scans leads to a total of about 21.4 mSv (2.13 rem), which is far less than the 50-mSv (5-rem) annual effective dose limit for WB imaging, as per title 21 of *Code of Federal Regulations*, part 361.1. WB dosimetry of ^{18}F -SP203 showed a higher dose to red marrow (30.9 $\mu\text{Sv}/\text{MBq}$) than that from other ^{18}F -labeled tracers, whereas the effective doses were similar (17.8 $\mu\text{Sv}/\text{MBq}$) (14).

The PET imaging method for dosimetry used in the current study, segmentation of each organ by threshold, has a strong advantage for the gallbladder, the urinary bladder, and other gastrointestinal organs over the CT-based traditional method, since the filling rate of pharmacokinetic uptake and the anatomic position will change over time with marked distension or movement (Wong lab, unpublished data).

The metabolism of ^{18}F -FPEB was not atypical, with the percentage metabolism in plasma being 75% and 80% at 30 and 90 min, respectively, and no lipophilic metabolites,

allowing a concrete characterization of the radioactivity plasma input function, although no preclinical studies of brain metabolites have been conducted. We confirmed that it is possible to routinely achieve specific activities at the end of synthesis of 2.2×10^5 to 2.96×10^5 MBq/ μmol (6–8 GCi/ μmol) and an average injected dose of about 185 MBq.

The evaluation of kinetic models indicated that PRGA might be a useful method for quantifying V_T , but it is premature to choose between PRGA and TTCM-C. Because the lowest V_T was in the pons, it may be an appropriate reference region for obtaining BP_{ND} with PRGA, whereas cerebellum is widely used for ^{11}C -ABP 688 (8). Volumes of distribution kinetic modeling using PRGA demonstrated that the V_T of the nondisplaceable compartment and BP_{ND} is consistent with that for human mGluR5. Most important, our test-retest variability in 5 human subjects was quite favorable and was less than 10% for most regions for BP_{ND} , in contrast to another mGluR5 PET radiotracer (40). Slightly higher test-retest variability estimates that we observed on V_T —including blood-brain barrier-related parameters—may not be a real issue in clinical applications of this radioligand when the preferred PET variable (BP_{ND} , not including these parameters) shows excellent reproducibility.

A comparison of FPEB with SP203 and ABP688 has been previously published (37). The high test-retest variability in humans with ^{11}C -ABP688 may make it a less than ideal ligand for receptor quantification (41). A possible disadvantage of FPEB may be the low radiochemical yield, although the amounts of tracer that can be synthesized are sufficient for human studies and, at Johns Hopkins University, are more than adequate for routine human PET studies.

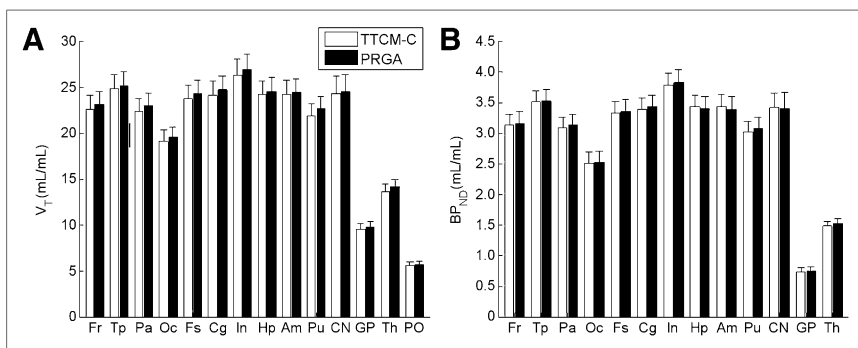


FIGURE 6. Histograms (means with SE bars, $n = 11$) of regional value of V_T (A) and BP_{ND} (B) given by TTCM-C and PRGA. Fr = frontal lobe; Tp = temporal lobe; Pa = parietal lobe; Oc = occipital lobe; Fs = fusiform gyrus; Cg = cingulate gyrus; In = insula; Hp = hippocampus; Am = amygdala; Pu = putamen; CN = caudate nucleus; GP = globus pallidus; Th = thalamus; PO = pons.

RGB

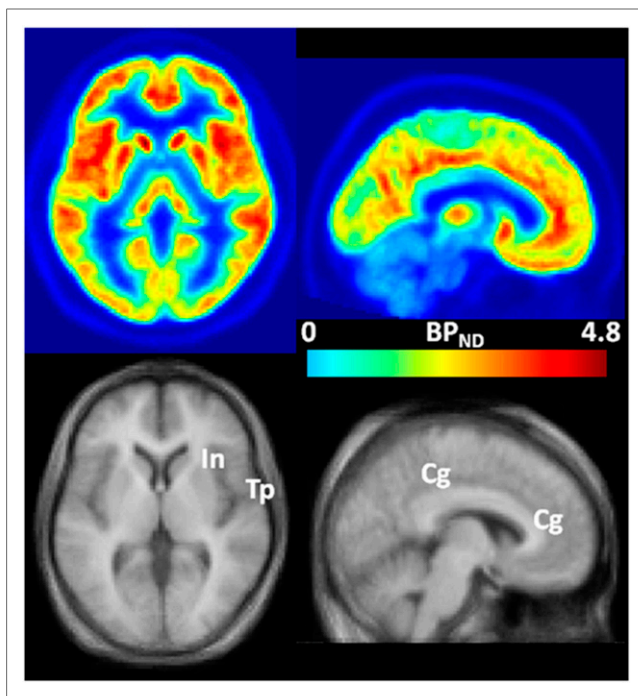


FIGURE 7. Transaxial (left) and sagittal (right) BP_{ND} images of ^{18}F -FPEB (top) and matching MR images (bottom) in SPM standard space. Regions with high BP_{ND} values, namely insular (In), temporal (Tp), and cingulate (Cg) cortices, are indicated on coregistered MR images.

Although mGluR5 occupancy was not evaluated in this pilot study, studies in nonhuman primates demonstrated that a 10 mg/kg dose of 3-[(2-methyl-4-thiazolyl) ethynyl] pyridine, an mGluR5 antagonist, nearly completely blocked regional brain uptake of this radiotracer in rhesus monkeys (12). Measurement of mGluR5 occupancy with therapeutic candidates is important and should be feasible with ^{18}F -FPEB. The use of mGluR5 human PET tracers for drug occupancy is increasingly relevant. For example, Novartis' AFQ056 (mGluR5 antagonist) has shown improvements in several Fragile X syndrome behavioral symptoms; STX 107, an mGluR5 blocker, for early testing of Fragile X, is being developed by Seaside Therapeutics; and RO4917523, another mGluR5 antagonist, is being developed by Roche. Given the good test–retest variability, ease of synthesis, and longevity of the ^{18}F label, there are considerable advantages in using ^{18}F -FPEB to study neuropsychiatric conditions and facilitate future drug development studies that include receptor occupancy.

CONCLUSION

PET scanning with ^{18}F -FPEB was shown in this first-in-human study to be safe and well tolerated, as all postscan clinical safety tests remained unremarkable. Regional brain uptake was consistent with known mGluR5 sites, and within-subject test–retest variability for most regions was favorable (<10%) for most brain regions. The initial quantification of BP_{ND} values and excellent test–retest estimates

strongly support the use of ^{18}F -FPEB in clinical imaging studies of mGluR5.

DISCLOSURE

The costs of publication of this article were defrayed in part by the payment of page charges. Therefore, and solely to indicate this fact, this article is hereby marked “advertisement” in accordance with 18 USC section 1734. This study was supported in part by NIH grants R33 MH66623P and K24DA000412 and by NIBIB, NIDA, NIAAA training grant 5T32EB006351-05 for clinician scientists in imaging research. Data from this study were presented in part at the Society of Nuclear Medicine annual meeting in San Antonio, Texas, on June 4–8, 2011. No potential conflict of interest relevant to this article was reported.

ACKNOWLEDGMENTS

We thank the staff members of the Johns Hopkins PET Center for their radiochemical syntheses and PET data acquisitions William Willis, Ayon Nandi, Emily Gean, Maria Guevara, Anil Kumar, Stephen Condouris, and Maria Thomas for technical support and coordination; Andrew Crabb and Arman Rahmin for High-Resolution Research Tomograph reconstruction and physics issues; and Drs. Igor Grachev and Richard Hargreaves from Merck for their collaboration and scientific advice. Changlae Lee and Hee-Joung Kim of Yonsei University, Wonju, Korea, contributed to the radiation dosimetry calculations. Parexel, Inc., accrued and cared for the subjects and performed most of the pharmacologic safety studies.

REFERENCES

1. Anwyl R. Metabotropic glutamate receptors: electrophysiological properties and role in plasticity. *Brain Res Rev.* 1999;29:83–120.
2. Bordi F, Ugolini A. Group I metabotropic glutamate receptors: implications for brain diseases. *Prog Neurobiol.* 1999;59:55–79.
3. Clewa RM, Olive MF. Positive allosteric modulators of type 5 metabotropic glutamate receptors (mGluR5) and their therapeutic potential for the treatment of CNS disorders. *Molecules.* 2011;16:2097–2106.
4. Simonyi A, Schachtman TR, Christoffersen GR. The role of metabotropic glutamate receptor 5 in learning and memory processes. *Drug News Perspect.* 2005;18:353–361.
5. Manahan-Vaughan D, Braunevell KH. The metabotropic glutamate receptor, mGluR5, is a key determinant of good and bad spatial learning performance and hippocampal synaptic plasticity. *Cereb Cortex.* 2005;15:1703–1713.
6. Palucha A, Pilc A. Metabotropic glutamate receptor ligands as possible anxiolytic and antidepressant drugs. *Pharmacol Ther.* 2007;115:116–147.
7. Christoffersen GR, Simonyi A, Schachtman TR, et al. mGlu5 antagonism impairs exploration and memory of spatial and non-spatial stimuli in rats. *Behav Brain Res.* 2008;191:235–245.
8. Ametamey SM, Treyer V, Streffer J, et al. Human PET studies of metabotropic glutamate receptor subtype 5 with ^{11}C -ABP688. *J Nucl Med.* 2007;48:247–252.
9. Siméon FG. Synthesis and simple ^{18}F -labeling of 3-fluoro-5-(2-(2-(fluoromethyl)thiazol-4-yl)ethynyl)benzotrile as a high affinity radioligand for imaging monkey brain metabotropic glutamate subtype-5 receptors with positron emission tomography. *J Med Chem.* 2007;50:3256–3266.
10. Shetty HU, Zoghbi SS, Siméon FG, et al. Radiodefluorination of 3-fluoro-5-(2-(2-[^{18}F](fluoromethyl)-thiazol-4-yl)ethynyl)benzotrile ([^{18}F]SP203), a radioligand for imaging brain metabotropic glutamate subtype-5 receptors with positron emission tomography, occurs by glutathionylation in rat brain. *J Pharmacol Exp Ther.* 2008;327:727–735.

11. Lucatelli C, Honer M, Salazar JF, Ross TL, Schubiger PA, Ametamey SM. Synthesis, radiolabeling, in vitro and in vivo evaluation of [¹⁸F]-FPECMO as a positron emission tomography radioligand for imaging the metabotropic glutamate receptor subtype 5. *Nucl Med Biol.* 2009;36:613–622.
12. Hamill TG, Krause S, Ryan C, et al. Synthesis, characterization, and first successful monkey imaging studies of metabotropic glutamate receptor subtype 5 (mGluR5) PET radiotracers. *Synapse.* 2005;56:205–216.
13. Treyer V, Streffer J, Ametamey SM, et al. Radiation dosimetry and biodistribution of ¹¹C-ABP688 measured in healthy volunteers. *Eur J Nucl Med Mol Imaging.* 2008;35:766–770.
14. Kimura Y, Simeon FG, Hatazawa J, et al. Biodistribution and radiation dosimetry of a positron emission tomographic ligand, ¹⁸F-SP203, to image metabotropic glutamate subtype 5 receptors in humans. *Eur J Nucl Med Mol Imaging.* 2010;37:1943–1949.
15. Bélanger MJ, Krause SM, Ryan C, et al. Biodistribution and radiation dosimetry of [¹⁸F]F-PEB in nonhuman primates. *Nucl Med Commun.* 2008;29:915–919.
16. International Commission on Radiological Protection. Recommendations of ICRP: ICRP publication 60. *Ann ICRP.* 1991;21:1–3.
17. Stabin MG, Sparks RB, Crowe E. OLINDA/EXM: the second-generation personal computer software for internal dose assessment in nuclear medicine. *J Nucl Med.* 2005;46:1023–1027.
18. Hilton J, Yokoi F, Dannals RF, Ravert HT, Szabo Z, Wong DF. Column-switching HPLC for the analysis of plasma in PET imaging studies. *Nucl Med Biol.* 2000;27:627–630.
19. Cristy M, Eckerman KF. *Specific Absorbed Fractions of Energy at Various Ages from Internal Photon Sources.* Oak Ridge, TN: Oak Ridge National Laboratory; 1987. Report ORNL/TM-8381/V1.
20. Foster DM. Developing and testing integrated multicompartment models to describe a single-input multiple-output study using the SAAM II software system. *Adv Exp Med Biol.* 1998;445:59–78.
21. Fischl B, van der Kouwe A, Destrieux C, et al. Automatically parcellating the human cerebral cortex. *Cereb Cortex.* 2004;14:11–22.
22. Patenaude B, Smith SM, Kennedy DN, Jenkinson M. A Bayesian model of shape and appearance for subcortical brain segmentation. *Neuroimage.* 2011;56:907–922.
23. Ashburner J, Friston KJ. High-dimensional image warping. In: Frackowiak RSJ, Friston KJ, Frith K, et al., eds. *Human Brain Function.* London, U.K.: Academic Press; 2003:673–694.
24. Maes F, Collignon A, Vandermeulen D, Marchal G, Suetens P. Multimodality image registration by maximization of mutual information. *IEEE Trans Med Imaging.* 1997;16:187–198.
25. Innis RB, Cunningham VJ, Delforge J, et al. Consensus nomenclature for in vivo imaging of reversibly binding radioligands. *J Cereb Blood Flow Metab.* 2007;27:1533–1539.
26. Berthele A, Platzer S, Laurie DJ, et al. Expression of metabotropic glutamate receptor subtype mRNA (mGluR1-8) in human cerebellum. *Neuroreport.* 1999;10:3861–3867.
27. Shigemoto R, Mizuno N. Metabotropic glutamate receptors immunocytochemical and in situ hybridization analyses. In: Ottersen OP, Storm-Mathisen J, eds. *Handbook of Chemical Neuroanatomy.* Vol 18. New York, NY: Elsevier; 2000:63–98.
28. Koeppe RA, Holthoff VA, Frey KA, Kilbourn MR, Kuhl DE. Compartmental analysis of [¹¹C]flumazenil kinetics for the estimation of ligand transport rate and receptor distribution using positron emission tomography. *J Cereb Blood Flow Metab.* 1991;11:735–744.
29. Abi-Dargham A, Laruelle M, Seibyl J, et al. SPECT measurement of benzodiazepine receptors in human brain with iodine-123-iomazenil: kinetic and equilibrium paradigms. *J Nucl Med.* 1994;35:228–238.
30. Logan J, Fowler JS, Volkow ND, et al. Graphical analysis of reversible radioligand binding from time-activity measurements applied to [¹¹C-methyl]-(-)-cocaine PET studies in human subjects. *J Cereb Blood Flow Metab.* 1990;10:740–747.
31. Wang GJ, Volkow ND, Fowler JS, et al. Reproducibility of repeated measures of endogenous dopamine competition with [¹¹C]raclopride in the human brain in response to methylphenidate. *J Nucl Med.* 1999;40:1285–1291.
32. Soares JC, van Dyck CH, Tan P, et al. Reproducibility of in vivo brain measures of 5-HT_{2A} receptors with PET. *Psychiatry Res.* 2001;106:81–93.
33. Hirvonen J, Nagren K, Kajander J, Hietala J. Measurement of cortical dopamine D₁ receptor binding with [¹¹C]SCH23390: a test-retest analysis. *J Cereb Blood Flow Metab.* 2001;21:1146–1150.
34. Yasuno F, Sanabria SM, Burns D, et al. PET imaging of neurokinin-1 receptors with [¹⁸F]SPA-RQ in human subjects: assessment of reference tissue models and their test-retest reproducibility. *Synapse.* 2007;61:242–251.
35. Lundberg J, Halldin C, Farde L. Measurement of serotonin transporter binding with PET and [¹¹C]MADAM: a test-retest reproducibility study. *Synapse.* 2006;60:256–263.
36. Burns HD, Van LK, Sanabria-Bohorquez A, et al. [¹⁸F]MK-9470, a positron emission tomography (PET) tracer for in vivo human PET brain imaging of the cannabinoid-1 receptor. *Proc Natl Acad Sci U S A.* 2007;104:9800–9805.
37. Brown AK, Kimura Y, Zoghbi SS, et al. Metabotropic glutamate subtype 5 receptors are quantified in the human brain with a novel radioligand for PET. *J Nucl Med.* 2008;49:2042–2048.
38. Akaike H. A new look at statistical model identification. *IEEE Trans Automat Contr.* 1974;19:716–722.
39. International Commission on Radiological Protection. ICRP publication 80: recalculated dose data for 19 frequently used radiopharmaceuticals from ICRP Publication 53. *Ann ICRP.* 1998;28:47–83.
40. Kuwabara H, Chamroonrat W, Mathews W, et al. Evaluation of ¹¹C-ABP688 and ¹⁸F-FPEB for imaging mGluR5 receptors in the human brain [abstract]. *J Nucl Med.* 2011;52(suppl):116P.
41. DeLorenzo C, Kumar JS, Mann JJ, Parsey RV. In vivo variation in metabotropic glutamate receptor subtype 5 binding using positron emission tomography and [¹¹C]ABP688. *J Nucl Med.* 2011;31:2169–2180.